Highlights

Experimental study of an ultrasonic mist generator as an evaporative cooler

Pedro Martínez, Javier Ruiz, Íñigo Martín, Manuel Lucas

- Performance and cooling capacity of a new ultrasonic mist generator are explored.
- The mist generator exhibits a maximum average evaporative cooling efficiency of 65%.
- A maximum direct evaporative cooling efficiency of 83.7% is observed.
- A novel performance indicator to evaluate pre-cooling process uniformity is defined.
- Optimum operating conditions are obtained for efficient evaporative cooling process.

Experimental study of an ultrasonic mist generator as an evaporative cooler

Pedro Martínez*, Javier Ruiz, Íñigo Martín, Manuel Lucas

Departamento de Ingeniería Mecánica y Energía, Universidad Miguel Hernández, Avda. de la Universidad, s/n, 03202, Elche, Spain

Abstract

This paper presents an ultrasonic mist generator used as an evaporative precooler for condensers in air conditioning applications. Ultrasonic mist generators eliminate pressure loss at the inlet air stream to the condenser and allow controlling the characteristics of the water atomized droplets. A water mist generation unit has been designed, built and tested to assess its thermal performance and its water mist production capacity in terms of mass flow rate of atomized water and size distribution of the droplets generated. To evaluate the performance and cooling capacity of the water mist produced by the ultrasonic mist generator, a set of tests has been conducted on a test bench consisting mainly of a subsonic wind tunnel equipped with instrumentation and control devices to modify the operating conditions. A Sauter mean diameter $D_{3,2} = 13.2$ μm has been determined for the size distribution of the generated droplets and the range of water mist flow rates that the system can produce is between 0.11×10^{-3} and 0.52×10^{-3} kg/s. It has been found that, under many operating conditions, the evaporative cooling process is not homogeneous throughout the air flow, so a novel performance indicator called $\varepsilon_{\mathrm{LCP}}$ (local cooling performance) has been defined to specifically evaluate this phenomenon. A maximum direct evaporative cooling efficiency $\varepsilon_{\mathrm{DEC}} = 83.7\%$ is obtained for a water-to-air flow ratio $r_w = 0.35 \times 10^{-3}$ and air flow rate 630 m^3/h, and a maximum average evaporative cooling efficiency of $\varepsilon_{\mathrm{AEC}} = 65\%$ for $r_w = 2.41 \times 10^{-3}$ and air flow rate 630 m^3/h.

Keywords:
evaporative cooling, ultrasonic nebulizer, cooling efficiency

*Corresponding author
Email address: `pedro.martinez@umh.es` (Pedro Martínez)
URL: `www.umh.es` (Pedro Martínez)

Nomenclature

c_{pa}	specific heat at constant pressure of dry air (J kg^{-1} K^{-1})
c_{pv}	specific heat at constant pressure of water vapour (J kg^{-1} K^{-1})
D	diameter (m)
$D_{1,0}$	arithmetic mean diameter (m)
$D_{3,2}$	Sauter mean diameter (m)
D_{NM}	median droplet size for the number distribution (m)
D_{vf}	vapour diffusion coefficient (m^2 s^{-1})
h_{fg}	enthalpy of vaporization (J kg$_w^{-1}$)
M	molecular weight (kg kmol^{-1})
$\dot{m}_{ai}$	inlet air mass flow rate at the atomization chamber (kg s^{-1})
$\dot{m}_w$	mass flow rate of water mist (kg$_w$ s^{-1})
R	ideal gas constant (J kmol^{-1} K^{-1})
r_w	water mist to air mass flow ratio (-)
T	dry temperature (°C)
t_d	theoretical droplet lifetime (s)
T_{wb}	wet bulb temperature of moist air (°C)
T_{wi}	temperature of the water in the tank (°C)
V_t	average air flow velocity in the wind tunnel (m s^{-1})

Greek symbols

$\varepsilon_{\mathrm{AEC}}$	average evaporative cooling (%)
$\varepsilon_{\mathrm{DEC}}$	direct evaporative cooling or saturation efficiency (%)
$\varepsilon_{\mathrm{LCP}}$	local cooling performance (-)
μ	dynamic viscosity (kg m^{-1} s^{-1})
ω	humidity ratio of moist air (kg$_w$ kg$_a^{-1}$)
ρ	density (kg m^{-3})

Subscripts

a	air
w	water
in	inlet air flow
out	outlet air flow

Abbreviations

AER	average evaporation rate (%)
COP	coefficient of performance
TH$_i$	thermo-hygrometer probe

1. Introduction

Evaporative cooling techniques applied to the condenser of a refrigerating machine represent one of the most effective and immediately applicable solutions for improving the efficiency of domestic and commercial air conditioning systems worldwide. With these techniques it is possible to reduce significantly, mainly in countries with hot-dry climates, the energy demand and the high consumption peaks. Energy savings contribute to reducing the dependence on fossil fuel in any country and have a direct impact on its economic development and growth, as well as decreasing greenhouse gas emissions. A considerable amount of studies in the literature show the benefits of pre-cooling techniques applied to different air conditioning systems. There are different strategies to reduce the temperature of the air entering the condenser. The most widely studied systems can be classified into: evaporative packings or pads and spray or mist generators. For direct evaporative coolers, Martínez et al. [2] investigated how different thicknesses of cooling pads influenced the energy performance of a split-type air-conditioner. They found that the highest increase of 10.6% in the overall coefficient of performance (COP) was achieved by a thickness of about

100 mm. The main drawback of pre-cooling systems based on evaporative pads is the additional pressure drop produced in the condenser air stream. Furthermore, this effect is present even if pre-cooling is not activated. Pressure drop causes a reduction in the air flow rate through the condenser and a decrease in its ability to reject heat to the environment. This means an increase in the condensation pressure, an additional compressor consumption and a reduced cooling capacity of the air-conditioning system, [4]. When water is sprayed over the evaporative pads and pre-cooling is activated, the temperature drop of the intake air to the condenser far outweighs both effects, the pressure drop and the air flow rate reduction, and results in savings of energy consumed by the compressor. However, when the water injection is not activated, the evaporative pads still generate a pressure loss that penalizes the energy consumption in the compressor.

Compared with direct evaporative coolers, mist or deluge systems give further installation flexibility because of their low profile piping network and provide negligible flow resistance to the air stream. Yu et al. [5] analysed the cooling effectiveness of mist in pre-cooling condenser air for an air- cooled chiller. In a subtropical climate, pre-cooling the condenser air by mist brought an increase of 0.36–8.86% and 0.34–10.19% in the coefficient of performance of the chiller under the normal mode (conventional head pressure control) and the VSD mode (variable speed control for the condenser fans), respectively. However, the use of water spray or deluge can cause corrosion, scaling, and fouling on the heat exchanger bundles if water droplets are carried by the airstream to the heat exchanger bundles of the condenser. To avoid this, the system is required to evaporate all water in the airstream to prevent water droplet contact with the heat exchanger surface. Special wet media or spray nozzles may be required to meet the requirement. High-pressure nozzles provide small water droplets but at a higher cost. Water quality affects the performance of the nozzles and their maintenance cost, [6]. In view of the drawbacks found in current techniques for pre-cooling, a search for alternatives seems appropriate.

Applications of ultrasonic energy to enhance a wide variety of processes or to improve system efficiency have been explored in recent years. Yao [7] makes an overview of studies about the applications of ultrasound as a new technology in the field of Heating, Ventilation and Air-Conditioning (HVAC), including air humidification/dehumidification, desiccant regeneration, air cleaning, heat enhancement and fouling reduction of heat exchanger, defrosting or frost suppression for air-conditioner evaporator. They claim that, from a general point of view, all the effects produced by ultrasound could be interesting in applications involving heat or mass transport, decreasing both the external and internal transport resistances. Nie et al. [8] studied an indirect flash evaporative cooling enthalpy recovery technology used for building ventilation based on counter flow plate heat exchanger combing with ultrasonic atomizer. Humidification by ultrasonic atomization was used to cool the indoor exhaust air down to its wet bulb temperature, resulting in sensible heat transfer and moisture condensation from the outdoor supplied air, in order to achieve total heat recovery. Compared to conventional indirect evaporative cooling, the application of ultrasonic atomization improves the cooling effect by increasing the water mist evaporation area. The results showed that in hot and humid climate, up to 71% of total heat recovery efficiency could be achieved by the prototype unit, and more than 50% of the enthalpy recovered was contributed by moisture condensation in the outdoor supply air. Arun and Mariappan [10] developed an ultrasonic regenerative evaporative cooler coupled with a desiccant dehumidifier, consisting of several sets of dry channels and wet channels where heat exchange occurs by indirect evaporative cooling of water mist generated by an ultrasonic atomizer. In this chiller, the conventional hygroscopic layer commonly used to moisten the air was replaced by the water mist. The results showed a cooling capacity of 339.8 W, for 0.0488 kg/s air mass flow rate and 0.37 extraction ratio, and reached maximum values of 1.15 for wet-bulb effectiveness and temperature drop of up to 10°C.

Recently, Yao et al. [11] presented a review of the state-of-the-art of high-intensity ultrasound and its applications. They reviewed recent studies on the applications of high-intensity ultrasound which are considered as new processes in fluids and multiphase media. These include processes such as chemical reactions, drying/dehydration, welding, extraction, heat transfer enhancement, de-ice, enhanced oil recovery, droplet atomization, cleaning and fine particle removal. In relation to droplet atomization, they explained the ultrasonic atomization by the surface-wave theory and the cavitation theory. The authors do not specifically cite evaporative cooling as an application of ultrasound, denoting the little attention they have received to date.

The literature review revealed that ultrasound is a promising method to improve the design of evaporative pre-cooling systems. Ultrasonic mist generators eliminate pressure loss at the inlet air stream to the condenser and allow controlling the characteristics of the atomized water generation. This paper explores thermal performance and fluid dynamic flow patterns of an ultrasonic mist generator as an evaporative pre-cooler for a condenser in air conditioning applications. A prototype of water mist generator has been designed and built specifically for this pre-cooling application. As an experimental laboratory unit, it has been necessary to characterize its final mist production capacity in terms of mass flow rate of atomized water and size distribution of the droplets generated. It was important to determine the range of mass flow rates that this system is able to supply, as it is directly related to its air pre-cooling capacity. On the other hand, the droplet diameter dictates how fast-evaporated the atomized water will be once it comes into contact with the main air stream. For this application, it is interesting to have a droplet size small enough so that the atomized water evaporates before reaching the condenser. In theory, this system may have the same disadvantages as the spray nozzle or deluge systems: corrosion, scaling and fouling phenomena on the heat exchanger bundles. However, this ultrasonic atomization system is capable of producing smaller droplet sizes, with a similar power consumption as systems using high pressure spray nozzles. The smaller the droplet size the faster evaporation occurs, so it is expected that the severity of these drawbacks will also be reduced. Also the soft, low-velocity mist produced by the ultrasonic atomization system, which generates droplets with much lower speeds than those produced by the spray nozzle systems, contributes to limit these problems, allowing to increase the contact time of the droplets with the air and reducing the evaporative distance. Different ultrasonic mist generator operating conditions were studied in a properly equipped wind tunnel.

In short, this is a multidisciplinary research work that includes energy balances and assessment of thermal performance, determination of fluid dynamic flow patterns and study of the conditions of atomized water generation using electronic ultrasound transducers. Such an approach has not been reported in literature hitherto.

2. Materials and Methods

2.1. Experimental test facility

To evaluate the performance and cooling capacity of the water mist produced by the ultrasonic mist generator, a set of tests has been conducted on a redesigned test bench specifically adapted for this purpose. The test rig mainly consists of two components: a ultrasonic mist generator unit and a subsonic wind tunnel where evaporative cooling takes place.

The ultrasonic mist generator has been built with the appropriate dimensions and water atomization capacity to work in combination with the wind tunnel, within the range of incoming air flow rates that commonly take place in the operation of air-cooled condensers. The mist generator mainly consists of a compact mist maker device equipped with 10 ultrasonic transducers, immersed in a tank with a steady water level, where the water atomization process is properly controlled. Table 1 shows the technical specifications and operating conditions of the mist maker unit. The ultrasonic transducer is composed of a piezo-electric crystal coupled to a 16 mm diameter ceramic disc. When submerged in water, the transducer is capable of transforming high frequency electronic signals, typically ranging from 0.8 to 1.65 MHz, into high frequency mechanical oscillations on the disc. When the water attempts to follow the ceramic disc's movements, it is unable to keep up with the high-frequency oscillations. As a result, the water is detached from the disc on the negative oscillations and produces a transitory vacuum, where the water cavitates and changes into steam. Then on the positive oscillation, the steam water is driven by the high pressure wave through the water surface. In this adiabatic process a fine water mist is formed, with droplet diameters on the scale of a few tens of microns, which are easily incorporated into the air flow.

To control the amount of atomized water produced by the ultrasonic mist generator, it is possible to select the number of ultrasonic transducers operating simultaneously and also to regulate the rotation speed of a fan coupled to the tank. This fan generates the necessary positive pressure into the tank to drive the atomized water out of it. This speed control is carried out by using an Arduino UNO microcontroller board, programmed to make this adjustment by directly operating a potentiometer and displaying the updated rpm on the computer screen.

Table 1: Technical specifications and operating conditions of the mist maker unit.

10 Head Ultrasonic Mist Maker	
Number of atomizing cores	10
Ceramic core diameter	16 mm
Input voltage	DC 48 V
Maximum input power	20 W/core
Resonance frequency	1650 ± 50 kHz
Maximum atomization amount	2.5 l/h
Working water temperature	1 – 55 °C
Working water level	60 – 80 mm

The open-circuit, subsonic wind tunnel shown in Figure 1 was used to perform the ultrasound evaporative cooling experimental tests. The nozzle along the honeycomb baffle (anti-turbulence screen) adapted in the entrance (leftmost part of the tunnel), ensures uniform, stable velocity profiles of the air flow. The test section of the wind-tunnel is 5.3 m long with a cross section of 0.492×0.712 m. Figure 2 shows an schematic arrangement of the test section, with dimensions of the wind tunnel and location of anemometer and thermo-hygrometer probes.

The wind tunnel is built with transparent PET (polyethylene terephthalate) 0.6 mm thick sheets. Its structure is detachable and allows to quickly add or remove different types of test sections. Its transparent walls allow the direct visualization of the water mist flow and its evolution along the test section. This feature is essential in order to properly interpret the temperature and humidity measurement fluctuations registered in the different tests.

The induced draft air flow rate is driven by a 0.55-kW axial fan located at the exit of the tunnel, and was maintained at different levels by a Toshiba-Tosvert VF-nC1 variable-frequency drive. It allows to set different air flow speeds in the tunnel, ranging from 0-3 m/s. This results in a maximum available volumetric air flow rate of 3783 m^3/h. A full description of the experimental wind tunnel facility can be found in [12, 13, 14].

2.2. Experimental procedure

A number of tests have been carried out to assess the performance of the mist generator unit. Firstly, the water mist flow rate that the unit is capable of supplying has been studied. Tests have also been conducted to determine the drop size distribution generated in the atomization process. Finally, the cooling

Figure 1: Photographic view of the test rig: (a) subsonic wind tunnel, (b) test section, (c) nozzle, (d) diffuser, (e) data acquisition system, (f) ultrasonic mist generator and (g) structure of water mist stream.

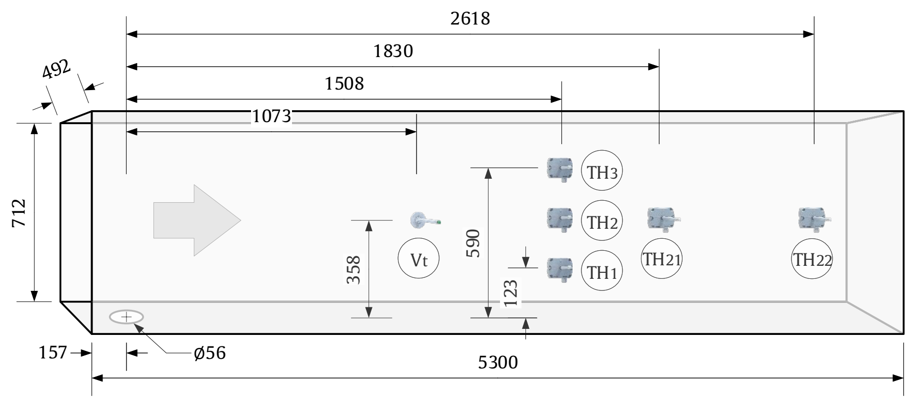

Figure 2: Schematic arrangement of the test section, dimensions of the wind tunnel and location of anemometer and thermo-hygrometer probes (dimensions in mm).

capacity of the water mist when injected into an airstream and the water mist distribution as a function of the air flow speed have been evaluated.

According to the UNE-EN 13741 standard [15], steady-state conditions have been maintained throughout the tests in the wind tunnel and in the mist generation process. The tests have been performed ensuring a maximum variation of ± 0.5°C in the inlet air flow temperature and $\pm 1\%$ in relative humidity. The water temperature supplied to the mist generator unit has been maintained in the same range of variation. The temperature and relative humidity probes have been calibrated by comparison to determine the zero error, before being installed in their final position. Prior to the commencement of each test, a start-up of all equipment is performed with a stabilisation period of at least 20 minutes. The readings of all the probes are considered stable when their fluctuations are in the range of the accuracy indicated by the manufacturer. To ensure the repeatability of the measurements, sensor readings have been taken at intervals of 10 seconds. The average values of each measurement have been made from a minimum of 50 readings taken consecutively.

Figure 3 shows the schematic layout and the different types of probes installed both on the wind tunnel and on the ultrasonic mist generator. Table 2 shows the technical specifications and accuracy of all the probes used in the tests. All measurements have been recorded with a Keysight 34970A data acquisition unit that incorporates three Keysight 34901A 20-channel-multiplexer modules.

2.3. Uncertainty analysis

An uncertainty analysis has been made according to the method proposed by Taylor and Kuyatt [16]. The associated uncertainty of the measurements for

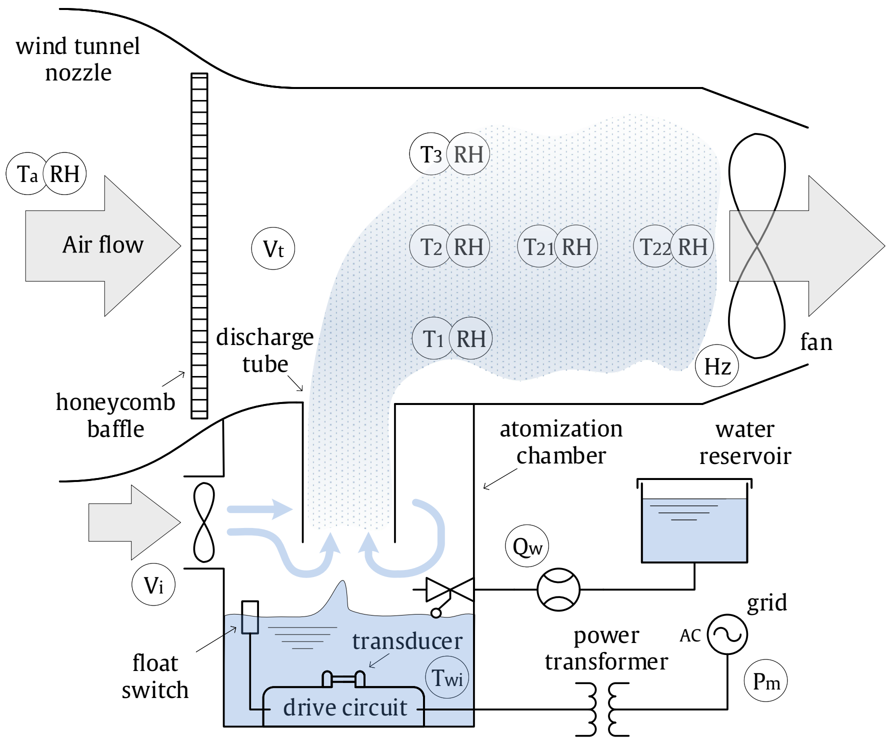

Figure 3: Schematic layout of the test rig showing the location of the probes and their corresponding type of measurement: (T) temperature, (RH) relative humidity, (V) air flow velocity, (Hz) power supply frequency, (Qw) water flow meter, (P) power consumption.

Table 2: Features and specifications of the probes used in the test rig.

Measurement	Measuring device	Brand	Model	Measuring range	Output signal	Accuracy
Air temperature	Thermo-hygrometer	E+E Elektronik	EE210-HT6xPBFxB	-20 to 80 °C	4–20 mA	± 0.2 °C
Air humidity	Thermo-hygrometer	E+E Elektronik	EE210-HT6xPBFxB	0–100% RH	4–20 mA	± (1.3+0.3% RD)% RH
Air temperature	Thermo-hygrometer	E+E Elektronik	EE210-HT6xPCxx	-20 to 80 °C	4–20 mA	± 0.2 °C
Air humidity	Thermo-hygrometer	E+E Elektronik	EE210-HT6xPCxx	0–100% RH	4–20 mA	± 2.5% RH
Air flow velocity	Anemometer	E+E Elektronik	EE65-VCD02	0–20 m/s	4–20 mA	± (0.2 m/s + 3% RD)
Air flow rate	Flow hood balometer	Testo	0563 4200	40–4000 m^3/h	USB port	± (12 m^3/h + 3% RD)
Power consump.	Power quality analyzer	Chauvin Arnoux	8334		USB port	± 1% RD
Water flow rate	Electromagnetic flowmeter	Krohne	OPTIFLUX 1050 C	0–10 m/s	4–20 mA	± (2.5 mm/s + 0.5% RD)
Water temperature	RTD-Pt100	Desin	ST-FFH PT100	-200 to 600°C	4-wires	± 0.05 °C
Water weight	Benchtop scale	PCE Instruments	PCE-TB 3	0–3 kg	4–20 mA	± 0.1 g

each probe is calculated using the following expression:

$$u_c = \sqrt{u^2_{\text{readout}} + u^2_{\text{datalogger}} + u^2_{\text{probe}}} \tag{1}$$

where u_c is the combined standard uncertainty of the probe; u_{readout} is the standard uncertainty associated with the repeatability of the probe readings; $u_{\text{datalogger}}$ is the uncertainty associated with the reading accuracy of the data acquisition unit; u_{probe} is the standard uncertainty associated with the calibrated accuracy of the probe. A value of 2 for the coverage factor k, corresponding to a level of confidence of approximately 95%, has been used to calculate the expanded uncertainty of each measurement. According to this uncertainty analysis, the maximum relative expanded uncertainties of the measurements taken with the probes have been calculated, the most important of which are: 0.2% in temperature, 2.3% in relative humidity and 3.4% in air flow velocity. From these values and the probe specifications shown in Table 2, a complete uncertainty analysis of the key performance indicators listed in Section 3.3.2 has been carried out. For this purpose, the uncertainty propagation command of the Engineering Equation Solver (EES) software and the well-known law of uncertainty propagation have been used:

$$U_{\text{KPI}} = k\sqrt{\sum_{i=1}^{N}\left(\frac{\partial f_{\text{KPI}}}{\partial x_i}\right) + u(x_i)^2} \tag{2}$$

where U_{KPI} is the expanded uncertainty of each key performance indicator, k is the coverage factor, f_{KPI} represents the definition equation of each indicator, $u(x_i)$ are the standard uncertainties of the variables or measurements on which the indicator depends (calculated for the probes according to the Equation (1)) and $\partial f/\partial x_i$ represents the sensitivity coefficients of these variables. The results of this uncertainty analysis for the key performance indicators are shown in Section 3.3.2.

3. Results and discussion

3.1. Measurement of the droplet size and distribution

This section shows the investigation that has been conducted to determine the droplet size and distribution produced by the mist generator unit. Three techniques have been tested in order to collect the droplets in different supports (sensitive papers, microscope slides) and subsequently estimate their diameters.

Firstly, the so-called sensitive paper technique has been used, as described in Ruiz et al. [17]. This involves placing water sensitive papers at the outlet of the discharge tube, causing the droplets of atomized water to impact onto the surface of the paper and leave a chemical mark on it.

The findings of this first test showed that this technique is not suitable for determining the size of droplets as small as those generated in the atomization chamber. The results are shown in Figure 4a, where it can be seen that the minimum droplet size that the kind of sensitive paper available in the laboratory is capable of registering, is approximately in the range of 60–80 μm in diameter.

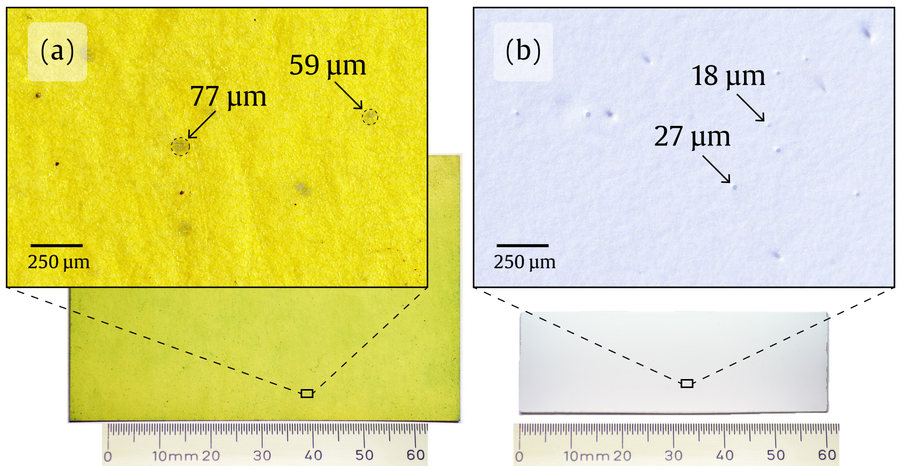

Figure 4: (a) Example of water sensitive paper and magnified view showing the minimum droplet size that this measurement technique is capable of recording. (b) Photograph of a magnesium oxide-coated slide and magnified view showing the smallest impacts that this technique is capable of capturing.

Secondly, the magnesium oxide technique has been used to record the droplets impact, as described by Chaskopoulou et al. [19]. This technique requires the deposition of a very thin layer of magnesium oxide on a microscope slide. In this way, when the droplets impact on the slide they form a crater that can be photographed to account for impacts and diameters. As with the previous method, this magnesium oxide technique was unable to visibly record the impacts of the atomized water droplets. Figure 4b shows the minimum droplet diameter that has been achieved using this technique, with the magnesium oxide layer deposition method described previously. The minimum diameter registered is in the range of 20–30 μm, a result somewhat above that reported by [19].

In view of the previous results, it was finally resolved to discard droplet impact techniques and to adopt a technique of direct photography of the droplets, similar to the method described by Ramisetty et al. [20]. With this photographic technique, it was possible to measure both the size and the velocity of the droplets generated in the ultrasonic atomization process. For this purpose, the droplets ejected through the discharge tube of the test rig have been photographed using a Pentax K-1 camera with a maximum shutter speed of 1/8000 s. A Tamron SP AF 90mm F2.8 Di Macro 1:1 lens is attached to the camera and an 18 cm extension tube is used to achieve higher lens magnification. Finally, a Pentax AF-360 FGZ auto flash unit has been used to freeze the droplet movement as they are ejected. The TTL flash mode is selected to achieve its fastest 1/2 peak duration time of approximately 1/20000 s. The photographs have been taken by arranging the flash on the opposite side of the camera position and using a remote trigger, whilst keeping the water mist flowing between the two devices. To simplify the photographic analysis it is necessary to reduce the number of droplets that appear in each shot. For this purpose, the light from the flash has been channelled through a 3 mm slit made by using a plastic sheet, with the objective of producing a narrow illumination plane to isolate the droplets. Only the droplets that pass through that illumination plane will be captured by the camera. An f-stop number of f/2.8 has been used in the camera to boost the isolation of the droplets captured in the shots, producing a very pronounced blurring of the droplets that are out of focus, which allows not to be counted in the subsequent photographic analysis. Photos taken with the camera have a native resolution of 7360 $\times$ 4912 pixels and have been processed with a graphic editor to increase contrast and acutance. The uncertainty of this measurement method is estimated by considering a variation of ± 1 pixel in the measurement of the droplet diameter by means of the digital image processing. Taking into account the native resolution of the camera and the magnification factor of the lens, the maximum uncertainty is estimated at $\pm 1.6 \mu$m. In Figure 5 there is an example of high shutter speed photography where the droplets movement is freezed and diameter measurements can be made.

Figure 6 shows a side view of the illumination plane made with a low shutter speed shot, where the light trails of the droplets can be clearly seen. The droplet velocity can be estimated by dividing the light trail length by the camera's shutter speed (in the case of continuous lighting) or by the flash duration. An image analysis technique has been used to measure the droplet size using the ImageJ and Fiji software. To estimate the droplet diameter, the two-dimensional circular area registered in the photographs and a sphericity filter ranging from 0.8 to 1 have been used to minimize the measuring error. Figure 7 shows the results of the droplet size and distribution. As can be seen, the arithmetic mean diameter of the droplets produced by the mist generator under the testing conditions is approximately $D_{1,0} = 8.1$ μm and the calculated Sauter mean diameter $D_{3,2} = 13.2$ μm. The arithmetic mean diameter ($D_{1,0}$) of the droplets produced by the mist generator and the Sauter mean diameter ($D_{3,2}$) were calculated according to the general mean diameter expression from the following equation:

$$D_{p,q} = \left[\frac{\sum_{i=1}^{N} n_i d_i^p}{\sum_{i=1}^{N} n_i d_i^q} \right]^{\frac{1}{p-q}} \tag{3}$$

where n_i represents the number of droplets with a diameter d_i.

Droplet diameter measurements are fairly in accordance with the results provided by other authors using more precise methodologies, such as the shadowgraphy technique [21] or the laser diffraction method [22].

The results are in accordance with the well-known equation that relates the

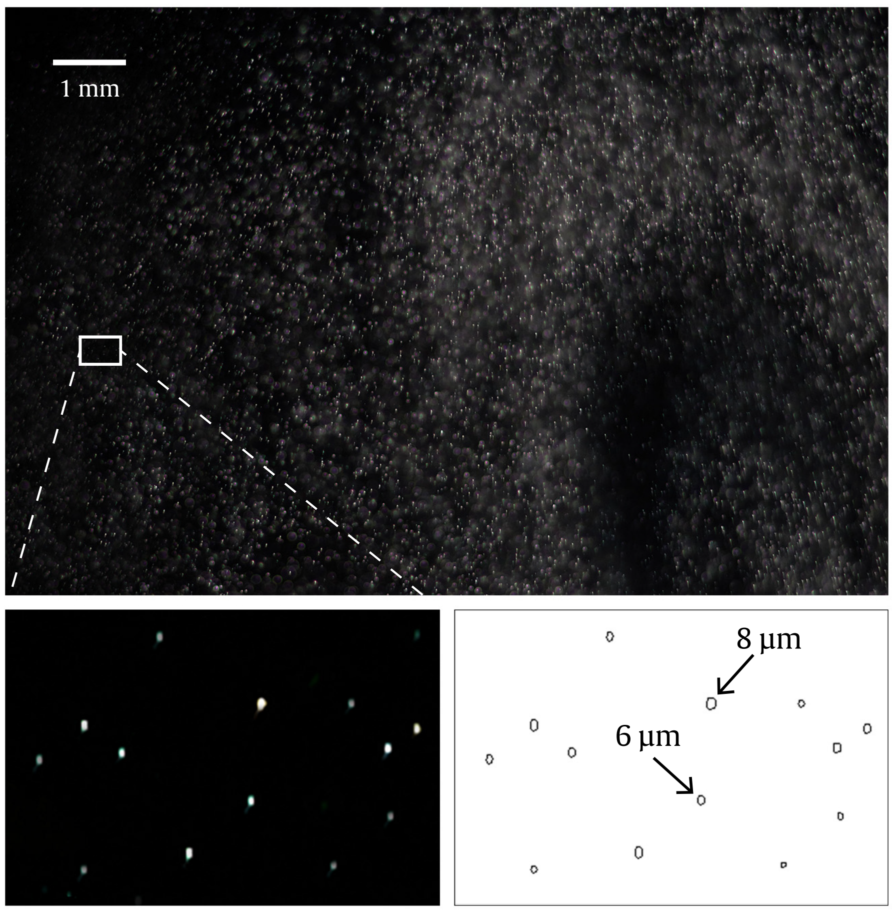

Figure 5: Example of high shutter speed photography that shows the droplet size and distribution.

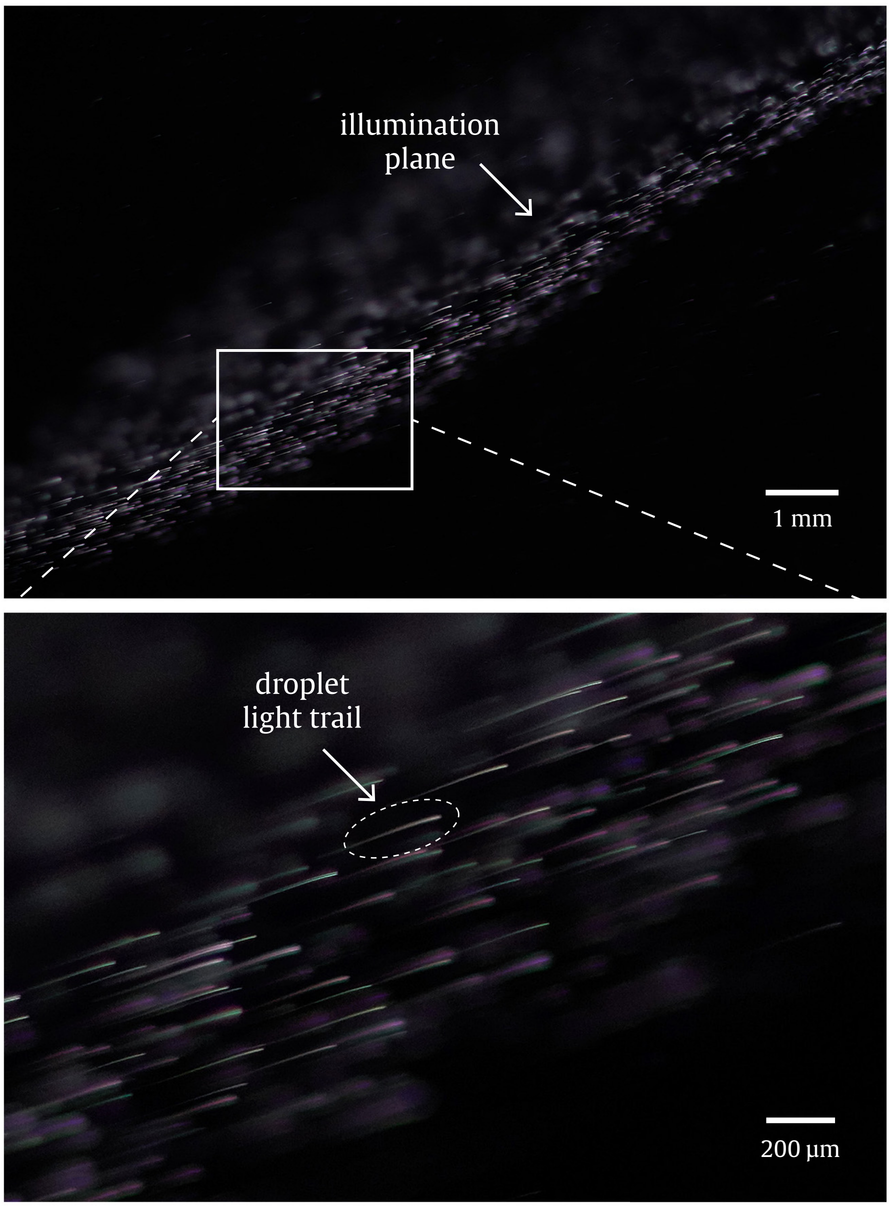

Figure 6: Low shutter speed photography and magnified view showing the illumination plane and the light trails of the droplets.

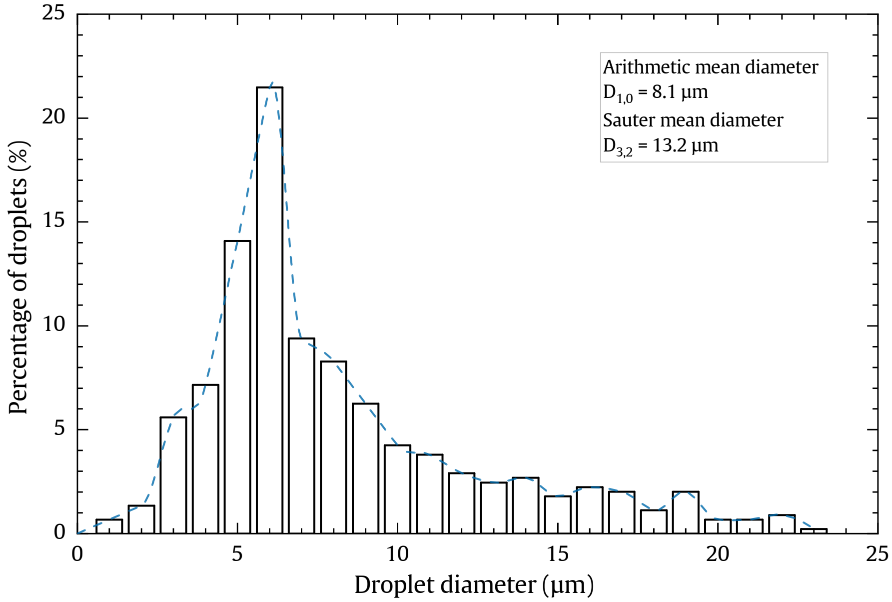

Figure 7: Droplet size and distribution measured at the outlet of the discharge tube.

droplet diameter to the water properties [22]:

$$D_{\mathrm{NM}} = \alpha_g \left(\frac{8\pi\sigma_s}{\rho_s} \right)^{1/3} F^{-2/3} \tag{4}$$

where $D_{\mathrm{NM}} = 6$ μm represents the median droplet diameter for the number distribution (not volume), α_g is a dimensionless constant of the mist generator, σ_s is the surface tension of the water, ρ_s is the water density and F is the resonance frequency of the piezo-electric crystal, approximately 1.6 MHz for the mist maker device. From this equation, a constant $\alpha_g = 0.67$ can be estimated for this mist generator, quite similar to the value of $\alpha_g = 0.65$ reported by [22] for this class of nebulizers. This small value of the droplet diameter justifies that the previous techniques based on the impact of droplets on a support could not be successfully applied. The results also show a characteristic droplet size distribution due to two main factors. On the one hand, there is the characteristic size dispersion that is generated in the environment of the ultrasonic transducers, where a significant agitation of the water surface takes place. On the other hand, there is the effect of droplet growth by coalescence, which depends on how long the droplets are retained in the atomization chamber before leaving through the discharge tube. The results shown in Figure 7 represent the average conditions established during the tests.

3.2. Water mist flow measurement

Prior to conducting the thermal performance tests on the water mist generator, it was necessary to characterize the range of the atomized water flows that the generator is capable of providing. The atomized water flow depends mainly on two variables: the air inlet velocity in the atomization chamber and the number of transducers operating simultaneously. For the purposes of thermal performance tests, it is interesting to have the maximum possible flow rate to produce a noticeable evaporative cooling in the air flow. For this reason, all the transducers were in operation simultaneously during the water mist flow measurement tests and only the incoming air velocity in the atomization chamber was changed. To adjust the velocity, the fan is provided with adjustable rotation speed selectable through the action on a potentiometer.

Two main methods of measuring the water mist flow rate have been considered in the tests: a volumetric method and a gravimetric method. Firstly, the volumetric method was used, which consists of calculating the water mist flow rate by measuring the descent of the water level inside the atomization chamber when the make-up water supply valve is closed. By measuring the variation in the water level and the dimensions of the container, the volume of evaporated water in a given time can be calculated; the mass flow rate is then calculated taking into account the temperature T_{wi} of the water in the tank. As there is no water supply during the tests, the duration of the tests is limited so as not to significantly change the water level over the ultrasonic transducers and therefore their response. A slanted tube manometer has been connected to the atomizing chamber, to easily visualize the water level inside the chamber. The water level in the tank is measured by visual inspection, by levelling the meniscus that forms the water on a millimetre scale. In order to increase the measurement accuracy, the tube has been arranged with an inclination of 21° above the horizontal. Tests have been completed with five levels of air flow velocity set by the fan and the results are shown in Figure 8. As shown in the figure, the uncertainty associated with this method of measurement is relatively high, mainly due to the visual error committed when reading the water level.

In order to improve these results, the gravimetric method has finally been used, which consists of measuring the weight of the supply water in a known time interval. In this case the water reservoir has been placed on a PCE-TB-3 benchtop scale and water weight measurements have been taken before and after each test. With this method, a direct measurement of the water mist mass flow rate is obtained. Figure 8a shows the comparison of the results obtained with both methods, showing the reduced uncertainty of the gravimetric method. Figure 8b shows the correlation between water mist mass flow rate and the velocity V_i of the air flow propelled into the atomization chamber. As can be seen, the different water mist flow rates that the system can produce are in the range of 0.11 to 0.52 g/s. In addition, the interpolated water mist production curve has an asymptotic character. This suggests that the maximum flow of water mist that the system can produce is being virtually extracted.

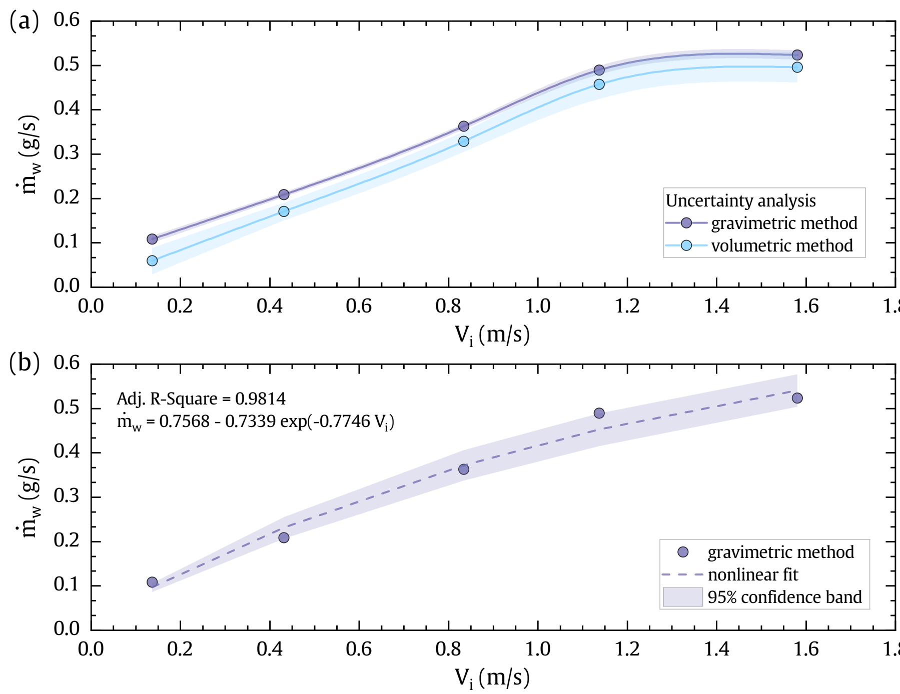

Figure 8: Water mist mass flow rate as a function of the velocity of the air flow propelled into the atomization chamber: (a) comparison and associated level of uncertainty between the results provided by the volumetric method and the gravimetric method; (b) computed correlation for the results of the gravimetric method.

3.3. Thermal performance and flow patterns

3.3.1. Test conditions and results

The evaporative cooling capacity of the atomized water flow produced by the mist generator has been evaluated through a set of tests. Additionally, an attempt has been made to identify the flow patterns that result when different mass flow rates are set for air flow and water mist flow. From a fluid dynamic point of view, the mixing process of the water mist into the air stream takes place according to a turbulent plume pattern of water mist.

A stable reference temperature of 25°C and relative humidity of 52% have been maintained throughout the tests for the inlet air flow. The parameters that have been varied in the experimental tests are the operating conditions that most affect the performance of the pre-cooling process: average air flow velocity (or equivalently, air flow rate) and mass flow rate of sprayed water mist. The average air flow velocity in the wind tunnel was calculated by a correlation between the measured instantaneous velocity in the middle of the cross-section and the actual volumetric air flow rate through the tunnel. This correlation was achieved from a prior air flow calibration test using measures from a balometer.

In practical cases of pre-cooling of the incoming air flow in low to medium power range air-cooled condensers, the average air flow velocity through the condenser is usually in the range of 0.5 to 2.5 m/s, and most commonly 1 to 1.5 m/s. Accordingly, four levels of air flow velocity have been considered: 0.5, 1.0, 1.6 and 2.2 m/s. This variation in average velocity corresponds to an equivalent range of air flow rates between 700 and 2760 m^3/h. Five additional levels of mass flow rate of sprayed water mist, ranging from 0.11×10^{-3} to 0.55×10^{-3} kg/s, have been considered for the tests. The total number of finally conducted tests was equal to 20. Table 3 shows a summary of the experimental measurements registered in some selected probes for all the tests that were conducted.

Table 3: Summary of experimental measurements registered on selected probes in the tests carried out.

V_t (m/s)	$\dot{m}_w$ (kg/s)	T_a (°C)	RH_a (%)	T_{TH1} (°C)	RH_{TH1} (%)	T_{TH2} (°C)	RH_{TH2} (%)	T_{TH3} (°C)	RH_{TH3} (%)
0.51	0.12×10^{-3}	24.9	55.5	22.4	69.2	24.5	54.4	24.8	53.7
	0.27×10^{-3}	24.8	55.2	21.9	73.1	22.4	68.7	24.9	53.0
	0.39×10^{-3}	25.0	54.2	21.9	73.1	20.7	83.5	22.6	67.8
	0.47×10^{-3}	25.4	53.4	21.9	74.3	20.5	85.7	20.6	87.0
	0.54×10^{-3}	25.3	53.6	23.1	65.4	20.7	86.0	20.1	94.5
1.05	0.14×10^{-3}	25.5	53.2	23.9	62.9	25.3	51.9	25.4	51.5
	0.27×10^{-3}	25.6	52.6	21.7	81.4	25.4	50.9	25.7	49.9
	0.41×10^{-3}	25.5	53.1	21.2	83.0	23.3	65.1	25.6	50.4
	0.49×10^{-3}	25.6	52.0	22.9	67.0	20.9	82.5	25.5	50.9
	0.53×10^{-3}	25.5	52.7	23.5	61.2	21.3	79.7	23.8	60.9
1.60	0.18×10^{-3}	25.9	51.6	24.3	58.8	25.6	50.7	25.8	50.1
	0.31×10^{-3}	26.0	51.8	21.6	82.0	25.6	50.6	25.9	49.7
	0.42×10^{-3}	25.9	52.0	20.3	93.9	25.4	52.0	26.0	49.6
	0.50×10^{-3}	25.8	51.8	20.4	90.3	23.7	62.3	25.9	49.5
	0.54×10^{-3}	25.9	50.9	21.7	78.0	21.4	78.9	25.9	49.2
2.18	0.21×10^{-3}	25.7	51.9	24.9	54.5	25.9	49.5	26.0	49.3
	0.32×10^{-3}	26.1	50.7	22.5	72.3	25.9	49.1	26.0	48.8
	0.43×10^{-3}	26.2	51.3	20.3	93.1	25.9	49.6	26.1	49.2
	0.51×10^{-3}	25.8	52.2	20.1	94.8	25.6	51.5	26.0	50.0
	0.55×10^{-3}	26.2	51.5	20.5	90.3	23.5	64.4	26.0	50.4

Figures 10–13 show graphically the results of these tests. The measured temperature and relative humidity variations collected by the thermo-hygrometers TH1, TH2 and TH3, located in the control section, 150 cm downstream from the outlet of the discharge pipe, are shown in Figure 3. Furthermore, Figure 9 shows the results of a preliminary test where it can be seen the temperature drop and the increase of specific humidity of the air, as it passes through the thermo-hygrometers TH2, TH21 and TH22, located on an axial axis in the centre of the wind tunnel. According to this last figure, the maximum temperature drop occurs when the water mist has covered an axial distance of approximately 1.5 m. Exactly in this position is where the thermo-hygrometers of the control section have been placed to carry out the rest of the tests.

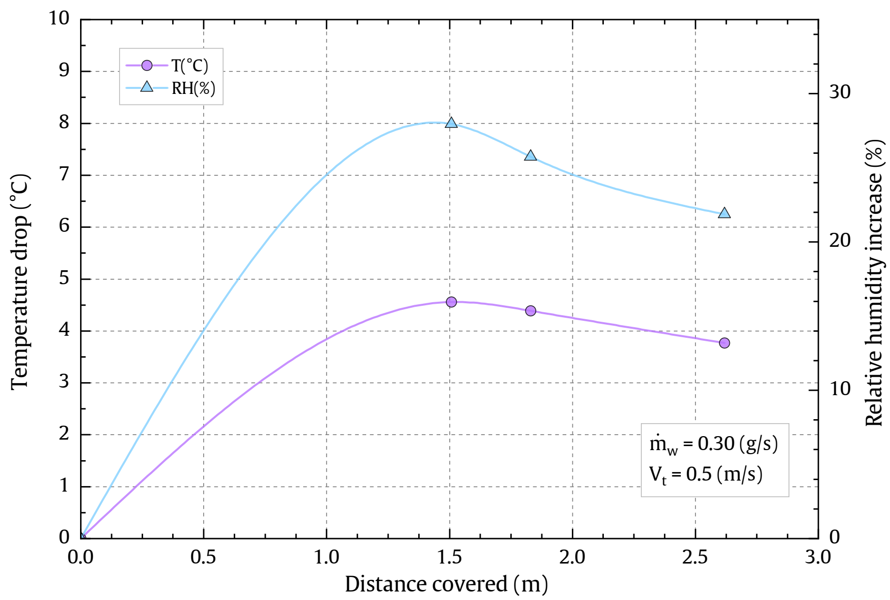

Figure 9: Temperature drop and relative humidity increase measured on the central axis of the wind tunnel as a function of the distance to the water mist discharge tube.

Figure 10 shows the results for an average air flow velocity of 0.5 m/s, corresponding to a flow rate of 630 m^3/h. With respect to the temperature registered by TH1, a drop of about 2.5°C compared to the ambient temperature can be seen when the lowest water flow is sprayed. This drop in temperature is even greater when the flow of water mist is increased. However, for TH2 and TH3 there is no noticeable change in temperature when the lowest flow of water mist is sprayed. This suggests that the sprayed water mist is dragged by the air flow velocity and the atomized droplets path seems to take a parabolic shape, with the dominant component of the velocity in the axial direction of the tunnel. The droplets trajectories do not reach the height position of TH2 and TH3 and, therefore, there is no variation in their measurements. As the flow of water mist increases, it is observed that the thermo-hygrometers TH2 and TH3, located at higher levels, begin to register a decrease in temperature. However, it is also observed that the thermo-hygrometer TH1 begins to measure a higher temperature when the water flow is maximum, because the droplets trajectories now do not impact it so directly. This indicates that, even with high flows, the plume of water mist is not uniformly distributed along the entire section of the tunnel. With regard to relative humidity measurements, the same results are observed for water mist distribution and a similar discussion can be made. Figure 14 shows the evolution of temperature and relative humidity measurements for the TH2 thermo-hygrometer, located at the center of the control section, for different air velocities and mass flow rates of sprayed water mist. The thermo-hygrometers that are not affected by the water mist plume do not register any variation in their relative humidity and maintain the environmental humidity of about 52%.

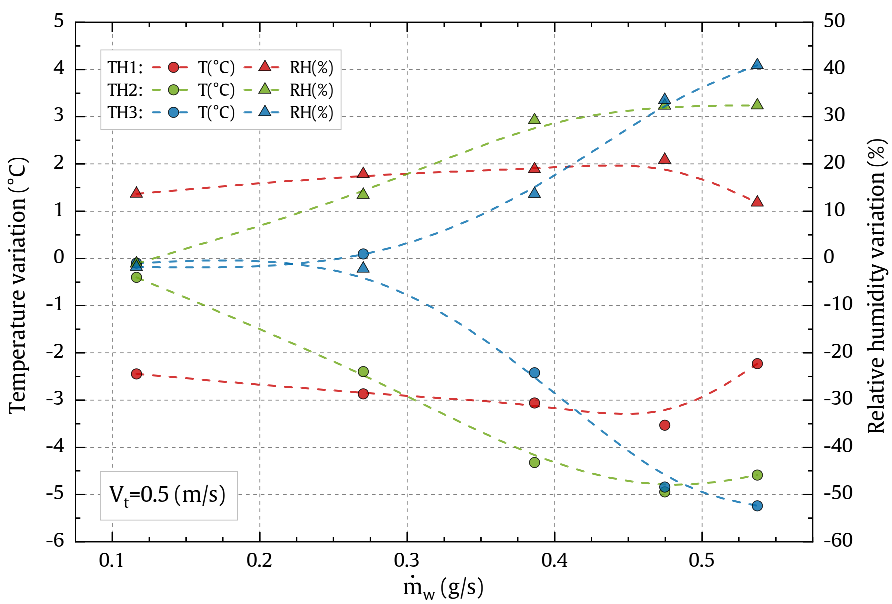

Figure 10: Temperature and relative humidity measured at the control section for an average air velocity of 0.5 m/s and different mass flow rates of sprayed water mist.

From the analysis of the results shown in the graphs it is possible to establish the flow pattern of the water mist plume inside the tunnel. Figure 13 very clearly illustrates the effect of increasing the air flow velocity. In this scenario, the axial component of the droplet velocity is predominant over its tangential component and the plume of water mist is practically trapped at the bottom of the wind tunnel. Virtually only TH1 detects variations in both temperature and relative humidity when the water mist flow is increased.

In Figure 15 a flow pattern interpretation of the results of Figure 13 has been

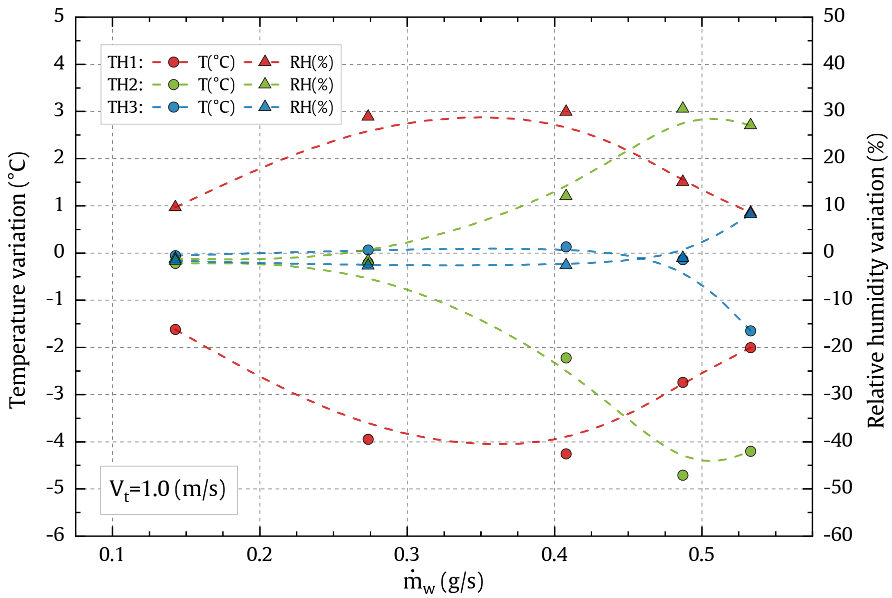

Figure 11: Temperature and relative humidity measured at the control section for an average air velocity of 1.0 m/s and different mass flow rates of sprayed water mist.

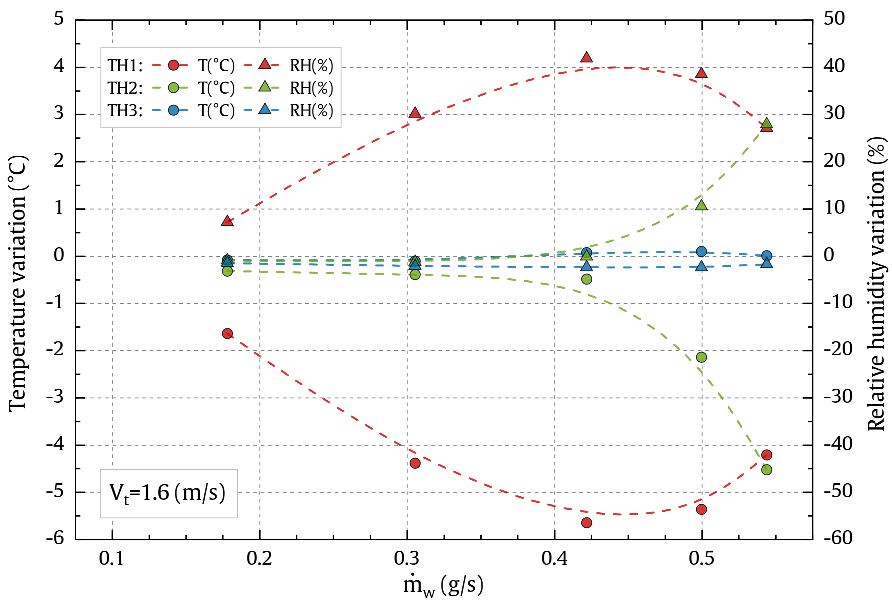

Figure 12: Temperature and relative humidity measured at the control section for an average air velocity of 1.6 m/s and different mass flow rates of sprayed water mist.

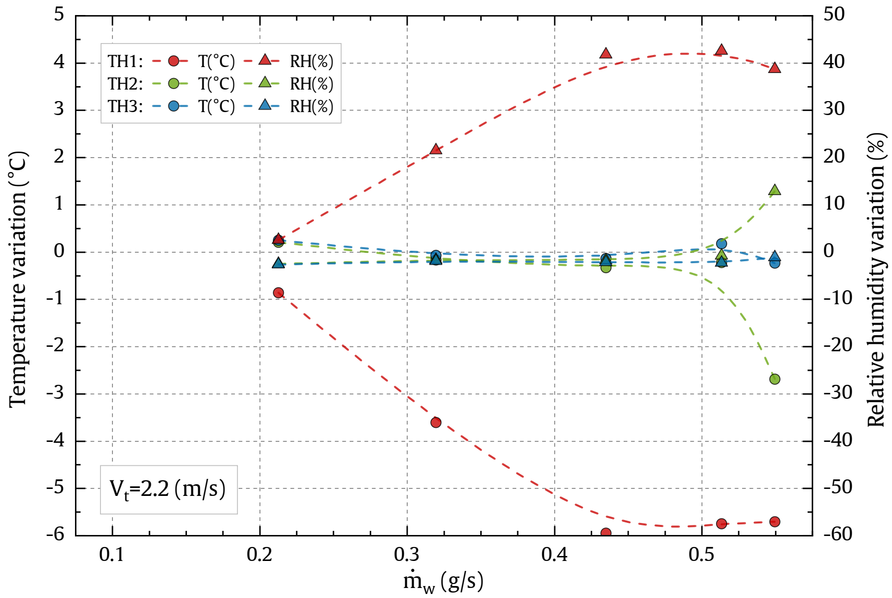

Figure 13: Temperature and relative humidity measured at the control section for an average air velocity of 2.2 m/s and different mass flow rates of sprayed water mist.

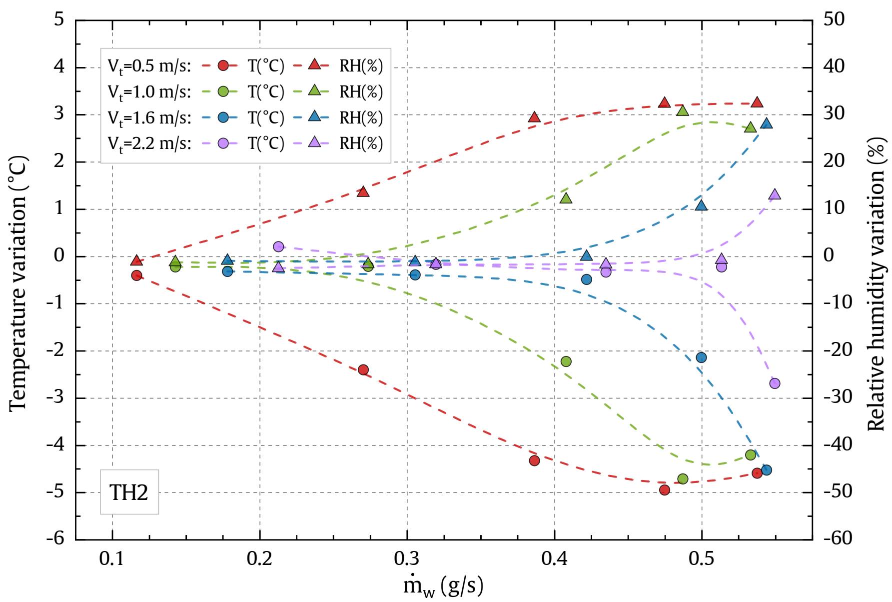

Figure 14: Temperature and relative humidity measured for the TH2 thermo-hygrometer, located at the center of the control section, for different air velocities and mass flow rates of sprayed water mist.

made. The evolution of the flow patterns of the water mist plume is shown as the water mist flow increases. The results in this particular scenario show a narrow plume flow pattern that is not suitable for achieving a uniform distribution of the evaporative cooling process. In the following section, the optimal operating conditions will be examined in order to obtain a more uniform distribution of this flow pattern.

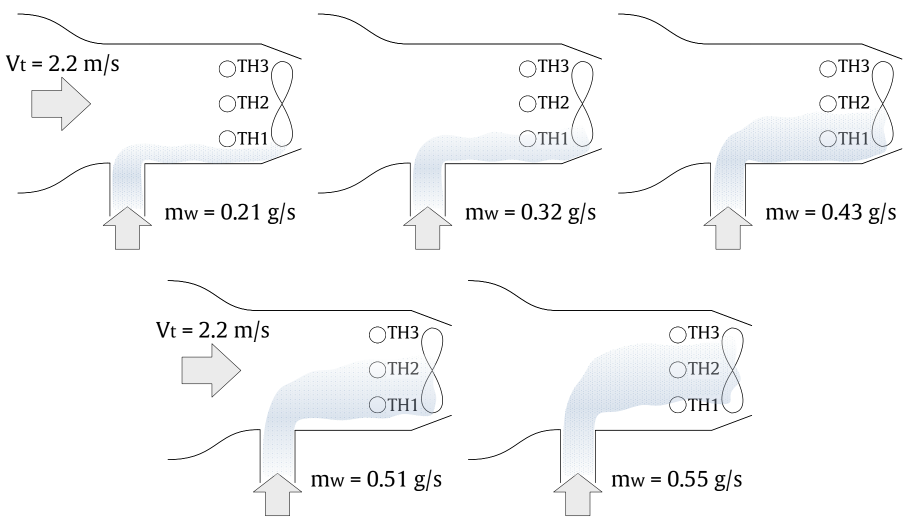

Figure 15: Schematic interpretation of the flow pattern as a narrow plume of water mist according to the results shown in Figure 13.

3.3.2. Key performance indicators (KPI)

The following performance indicators have been used to assess the thermal performance and the cooling capacity of the mist generator unit, with respect to different air and water mist input conditions.

r_w: water mist to air mass flow ratio

$$r_w = \frac{\dot{m}_w}{\dot{m}_a} \tag{5}$$

$\varepsilon_{\mathrm{DEC}}$: direct evaporative cooling or saturation efficiency, represents the extent to which the air flow temperature in a particular location (T_i), after a direct evaporative cooling process, approaches the wet bulb temperature (T_{wb}), defined as:

$$\varepsilon_{\mathrm{DEC}} = 100 \times \frac{T_a - T_i}{T_a - T_{wb}} \tag{6}$$

$\varepsilon_{\mathrm{AEC}}$: average evaporative cooling, represents the extent to which the average temperature of the air flow (T_{av}) approaches the wet bulb temperature (T_{wb})

of the incoming air or the extent to which it approaches complete saturation, defined as:

$$\varepsilon_{\text{AEC}} = 100 \times \frac{T_a - T_{av}}{T_a - T_{wb}} \tag{7}$$

ε_{LCP}: local cooling performance, denotes the extent to which the temperature in a particular region of the air flow (T_{THi}) approaches the minimum average temperature (T_{min}) that would be reached if all the water mist evaporates, defined as:

$$\varepsilon_{\text{LCP}} = \frac{T_a - T_{THi}}{T_a - T_{min}} = \frac{1}{r_w}\frac{c_{pa} + \omega_a c_{pv}}{h_{fg}}(T_a - T_{THi}) \tag{8}$$

AER: average evaporation rate, indicates the percentage of incoming water mass flow rate that has been evaporated when the plume of nebulized water reaches the control section, estimates as:

$$\text{AER} = 100 \times \frac{\dot{m}_{evap}}{\dot{m}_w} = 100 \times \sum_{i=1}^{6}\left(\frac{A_i}{A_T}\frac{1}{r_w}\frac{c_{pa} + \omega_a c_{pv}}{h_{fg}}(T_a - T_i)\right) \tag{9}$$

where T_i are the interpolated temperatures in the control section, A_T is the total cross-sectional area of the tunnel and A_i represents the circular sectors into which this section has been divided to calculate the average temperature

3.3.3. Thermal performance results

Figure 16 shows the direct evaporative cooling efficiency (ε_{DEC}) for all the tests carried out, calculated at the positions of the thermo-hygrometers TH1, TH2 and TH3, representing the three regions of the tunnel into which the analysis has been divided. Air and water mist flows have been more conveniently represented by the parameter r_w to facilitate the interpretation of the results. As can be seen in the figure, the saturation efficiency values are quite uneven, depending on if the water mist reaches the measuring region or not. Maximum local saturation efficiency reaches a value of 83.7%, with an expanded relative uncertainty of 4.9% for this performance indicator. Saturation efficiency behaves differently in the three regions examined. In the region corresponding to TH1, the highest values of saturation efficiency are obtained. As can be expected, the lower the r_w ratio, the higher the saturation efficiency value.

However, in Figure 16 it can be seen that the results in this region are scattered over a wide area (coloured in red), suggesting that the water mist plume has a fluctuating flow pattern. On the other hand, in the TH2 region the results show less dispersion and are grouped in a characteristic S-shaped green area. The figure indicates the threshold value of $r_w = 0.65 \times 10^{-3}$, above which the water mist begins to affect the TH2 region and increase its saturation

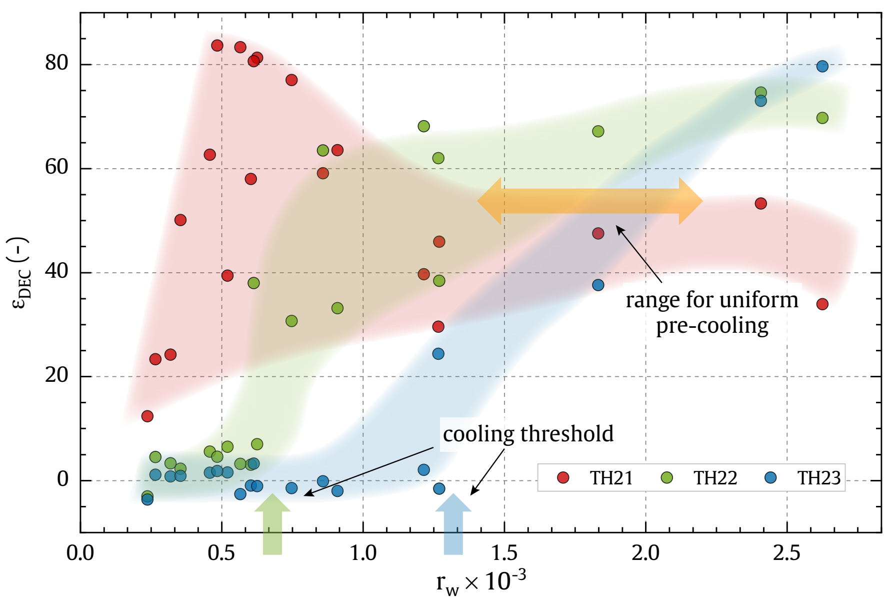

Figure 16: Direct evaporative cooling efficiency ($\varepsilon_{\mathrm{DEC}}$) calculated at positions TH1, TH2 and TH3 for all tests carried out. The highlighted range represents the water-to-air flow ratios that produce a more uniform distribution of the evaporative cooling effect.

efficiency. Finally, in the TH3 region a very low dispersion of results is obtained, grouped in a narrow blue area with a threshold value of $r_w = 1.35 \times 10^{-3}$ and a progressive increase of the saturation efficiency until reaching a maximum value of 79.7%. In view of the findings, Figure 16 indicates the range of r_w values that enables a more uniform distribution of the water mist over the entire wind tunnel section and more homogeneous evaporative cooling. This range is obtained by identifying in the graph the place where the intersection of the three colored areas almost occurs, yielding an estimated r_w range of 1.4×10^{-3} to 2.3×10^{-3}.

Figure 17 gives the local cooling performance ($\varepsilon_{\mathrm{LCP}}$) calculated in the three regions of the analysis and for all the tests carried out. As can be seen in the figure, the values of $\varepsilon_{\mathrm{LCP}}$ are scattered over a wide range from 0 to 5.2, with an expanded relative uncertainty of 9.6%. A horizontal line representing $\varepsilon_{\mathrm{LCP}} = 1$ has been plotted on the graph indicating the operating conditions that provide a local evaporative cooling equivalent to the average cooling of the entire control section. It is remarkable to note the very high values of $\varepsilon_{\mathrm{LCP}}$ that occur in the TH1 region, for low r_w flow ratios. These values indicate that the local cooling is up to 4 or 5 times higher than the average cooling. This behavior is compatible with the presence of a narrow plume flow pattern of water mist located near the bottom of the tunnel, which enhances evaporative cooling in that region. As in the previous case, the findings of this performance indicator can also be used to identify the range of r_w flow ratios that produce a more homogeneous distribution of water mist and evaporative cooling. In this case, the operating conditions resulting in a value of $\varepsilon_{\mathrm{LCP}} = 1$ are the most suitable for obtaining homogeneous evaporative cooling over the entire control section. As can be seen in the graph, the three regions analyzed are close to $\varepsilon_{\mathrm{LCP}} = 1$ in the range of r_w from 1.4×10^{-3} to 2.3×10^{-3}.

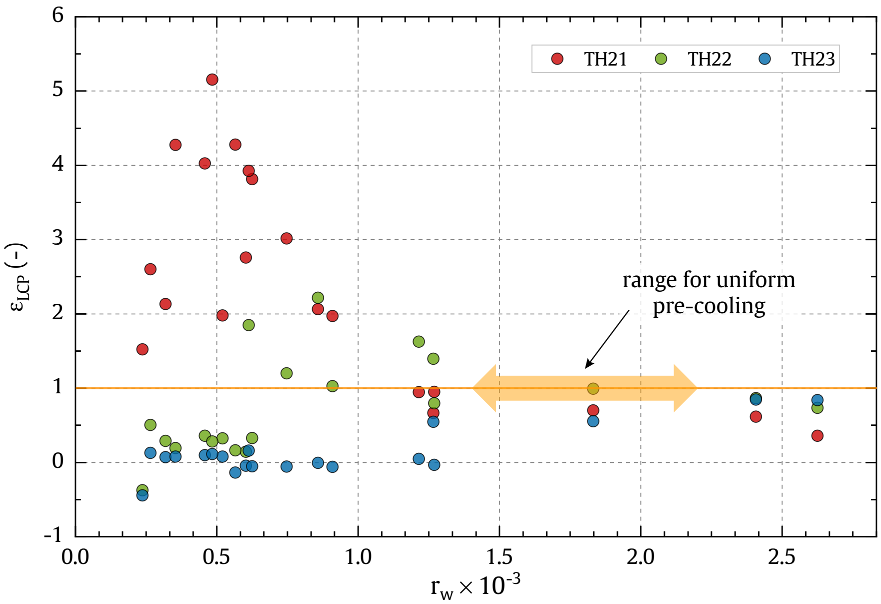

Figure 17: Local cooling performance ($\varepsilon_{\mathrm{LCP}}$) calculated at positions TH1, TH2 and TH3 for all tests carried out.The highlighted range represents the water-to-air flow ratios that produce a more uniform distribution of the evaporative cooling effect.

Finally, the utilization of the sprayed water mist has been evaluated through the average evaporation rate (AER). In this case, AER is a performance indicator that indicates the percentage of the water mist that has evaporated at a distance of 1.5 m from the discharge tube. AER has been estimated from an approximate average of the temperature distribution at the control section of the tunnel, so the values are not very accurate and have to be assessed from a qualitative point of view. This indicator informs whether the system has achieved its maximum evaporative cooling, when AER=100%, or whether the air flow will be further cooled beyond the control section. Similarly, this indicator provides information on the effective cooling distance, that is, the distance the water mist has to travel to evaporate completely and provide maximum evaporative cooling of the air flow. A theoretical calculation can be made of the distance that a droplet, with a known diameter, travels until it evaporates completely under certain ambient conditions. For this purpose one can use the Holterman's equation of a droplet lifetime [23]:

$$t_d = \frac{2}{q_1^2 q_0 \Delta T} \left[q_1 D_0 - \ln(1 + q_1 D_0)\right] \tag{10}$$

where D_0 is the initial droplet diameter, ΔT is the air wet-bulb depression and the rest of the terms are calculated with the following set of equations:

$$q_0 = \frac{8\gamma M_w D_{vf}}{\rho_w R T_a}(1 + bs_0) \tag{11}$$

$$q_1 = \frac{br_0}{1 + bs_0} \tag{12}$$

$$b = 0.276 \left(\frac{\rho}{\mu D_{vf}^2}\right)^{1/6} \tag{13}$$

$$D_{vf} = 22.5 \times 10^{-6} (\frac{T_a}{273.15K})^{1.8} \ [\mathrm{m}^2 \ \mathrm{s}^{-1}] \tag{14}$$

where M_w: molecular weight, ρ_w: density and μ_w: dynamic viscosity are water properties, T_a: air absolute temperature, D_{vf}: vapour diffusion coefficient, R: ideal gas constant, $\gamma = 67$ Pa/K, r_0=64.65 s$^{-0.5}$ and $s_0 = -1.117 \times 10^{-3}$ m s$^{-0.5}$

In the present study, with Sauter mean diameter $D_{3,2} = 13.2$ μm and ambient conditions of 25°C and relative humidity 52%, the use of the above equation gives a residence time of the droplets in the air of about $t_d = 0.26$ s. Considering the maximum air velocity achieved in the tests, the above result translates into an equivalent distance of 57 cm at which all the water droplets should theoretically evaporate. However, this result differs significantly from what was visually observed during the tests, where the plume of water mist reaches distances of more than 2 m before vanishing. This is partly explained by the concentration of droplets, when the plume has a small characteristic size, that makes the evaporation process more difficult and makes the droplet lifetime much longer. Figure 18 presents the average evaporation rate results evaluated in the control section for all tests performed. As can be seen, there is a wide range of evaporation rates from 43% to 92%. For the same air flow rate, AER generally increases as r_w increases. This is due to the higher droplet dispersion that produces a higher water flow, which makes the evaporation process easier.

Finally, Figure 19 shows the results of average cooling efficiency ($\varepsilon_{\mathrm{AEC}}$) calculated at the control section. The arrangement of the data suggests a clear dimensionless relationship between $\varepsilon_{\mathrm{AEC}}$ and r_w. As can be noticed, the highest values of this indicator are given for low air flow velocities, obtaining a maximum $\varepsilon_{\mathrm{LCP}} = 65\%$ for a flow rate ratio $r_w = 2.41 \times 10^{-3}$ and $V_t = 0.5$ m/s. In practical cases of pre-cooling of the incoming air flow in low to medium power range air-cooled condensers, the average air flow velocity through the condenser is usually in the range of 1 to 1.5 m/s. In this situation, the maximum efficiency of this

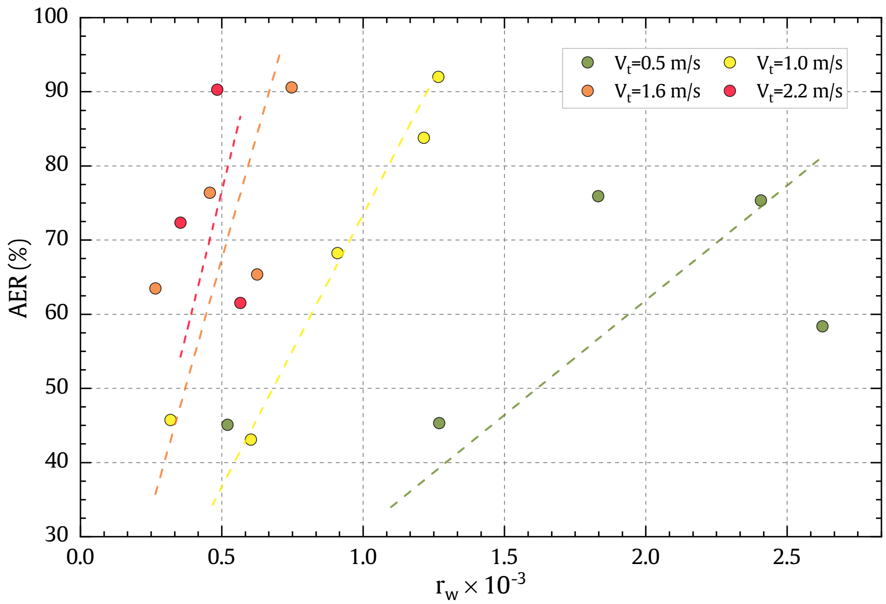

Figure 18: Percentual value of the average evaporation rate (AER) calculated at the control section for all tests carried out.

water mist system is close to 40%. Increased cooling efficiency can be achieved by providing a higher flow of water mist and more effective dispersion of the droplets in the air stream, to enhance their complete evaporation.

4. Conclusions

In this work, a water mist generation unit using ultrasonic transducers has been designed, built and tested for its behaviour and performance. The performance of this equipment to produce evaporative cooling in an air stream, under different test conditions established in a wind tunnel, has been investigated by means of different key performance indicators. The application of this system is aimed at increasing the performance of air conditioning systems, by means of evaporative pre-cooling of the incoming air flow into the air-cooled condensers. The literature review reveals virtually no studies on the use of ultrasonic nebulizers for pre-cooling processes on condensers. The most relevant results of this study are reported hereinafter:

- It has been found that the evaporative cooling process is not homogeneous throughout the air flow at many operating conditions, so a novel performance indicator called $\varepsilon_{\mathrm{LCP}}$ (local cooling performance) has been defined to specifically evaluate this phenomenon.

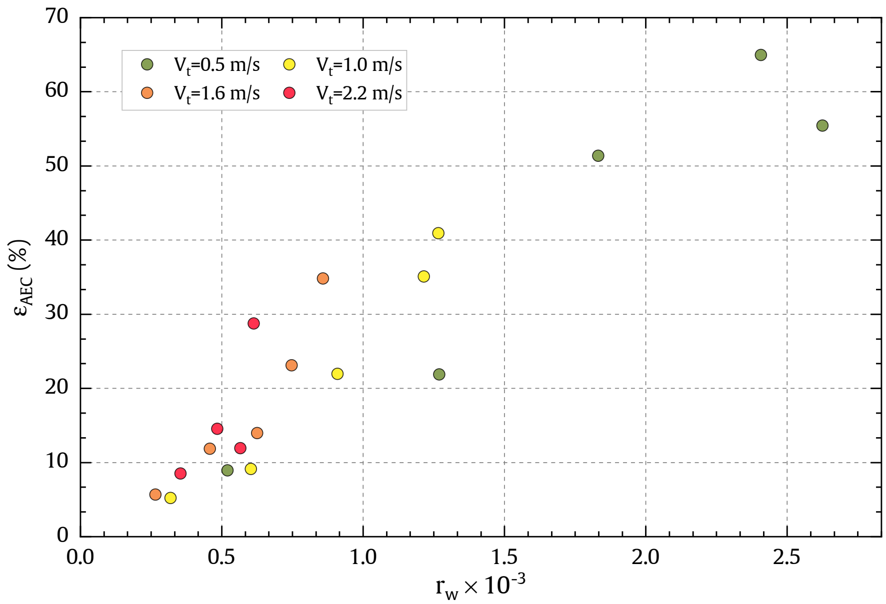

Figure 19: Average evaporative cooling efficiency ($\varepsilon_{\mathrm{AEC}}$) calculated at the control section for all tests carried out.

- The average evaporative cooling efficiency ($\varepsilon_{\mathrm{AEC}}$) increases when the atomized water flow is increased and the air flow rate is reduced, obtaining a maximum $\varepsilon_{\mathrm{AEC}} = 65\%$ for a water-to-air flow ratio $r_w = 2.41 \times 10^{-3}$ and air flow rate 630 m^3/h, and $\varepsilon_{\mathrm{AEC}} = 41\%$ when $r_w = 0.13 \times 10^{-3}$ and air flow rate 1261 m^3/h.

- The size and distribution of the water droplets that this equipment is capable of producing has been determined, resulting in a Sauter mean diameter $\mathrm{D}_{3,2} = 13.2\ \mu\mathrm{m}$.

- It has been identified that in the range of $r_w = 1.4\times10^{-3}$ to 2.3×10^{-3} there is a better distribution of the water mist throughout the control section and a more homogeneous and effective evaporative cooling process.

- The water atomization capacity of the system has been measured by a gravimetric method and the range of water flow rates that the system can produce is between 0.11×10^{-3} and 0.52×10^{-3} kg/s.

- A maximum direct evaporative cooling efficiency $\varepsilon_{\mathrm{DEC}} = 83.7\%$ is obtained for a water-to-air flow ratio $r_w = 0.35 \times 10^{-3}$ and air flow rate 630 m^3/h.

From the findings of this study, it is concluded that an ultrasonic mist generator is a promising alternative to conventional evaporative cooling systems based on cooling pads. This system can be used to pre-cool the incoming air flow in a condenser with the following advantages: there is no pressure loss in the air flow; no maintenance and cleaning or replacement of the evaporative pads is required; hydraulic circuit is simpler, no water recirculation is required and the water tank is significantly smaller; no accumulation of salts and other substances in the tank or in the cooling pads.

There are a number of issues that still need to be addressed in further research. In the future, we plan to optimize the design of the ultrasonic mist generation system from an energy perspective (minimizing electrical consumption and maximizing cooling capacity) along with minimizing the impact of droplets on the condenser heat exchanger. Another issue that has to be solved in the evaporative pre-cooling process is the difficulty of achieving homogeneous cooling in the whole air stream. It is therefore important to investigate other methods of water mist spraying. A possible extension of the research is to carry out a CFD based numerical simulation of the evaporative cooling phenomenon, to explore different geometries and operating conditions in order to enhance the pre-cooling process. Another area of interest is the energy and exergy efficiency analysis of the generation and use of water mist, with the objective of optimizing the use of ultrasound technology and even exploring other applications in the field of air conditioning.

Acknowledgements:

This research is funded by FEDER/Ministerio de Ciencia e Innovación – Agencia Estatal de Investigación throuhg Spanish research projects ENE2017-83729-C3-1-R and ENE2017-83729-C3-3-R, supplied by FEDER funds.

The authors wish to acknowledge the collaboration of E. Sánchez and recognize his amazing work as a lab technician. Anonymous reviewers have provided insightful comments that have helped improving the manuscript.

Conflicts of Interest:

The authors declare no conflict of interest. The funders had no role in the design of the study; in the collection, analyses, or interpretation of data; in the writing of the manuscript, or in the decision to publish the results.

References

[1] IEA, The Future of Cooling: opportunities for energy-efficient air conditioning, Annual report, International Energy Agency, Paris, 2018. doi:10.1787/9789264301993-en.

[2] P. Martínez, J. Ruiz, C. Cutillas, P. Martínez, A. Kaiser, M. Lucas, Applied Thermal Engineering 105 (2016) 1041 – 1050. doi:10.1016/j.applthermaleng.2016.01.067.

[3] N. I. Ibrahim, A. A. Al-Farayedhi, P. Gandhidasan, Applied Thermal Engineering 110 (2017) 1255 – 1263. doi:10.1016/j.applthermaleng.2016.09.042.

[4] M. Mehrabi, D. Yuill, International Journal of Refrigeration 85 (2018) 409 – 430. doi:10.1016/j.ijrefrig.2017.10.017.

[5] F. Yu, W. Ho, K. Chan, R. Sit, Applied Thermal Engineering 130 (2018) 112 – 119. doi:10.1016/j.applthermaleng.2017.11.046.

[6] K. Hooman, Z. Guan, H. Gurgenci, in: M. J. Blanco, L. R. Santigosa (Eds.), Advances in Concentrating Solar Thermal Research and Technology, Woodhead Publishing Series in Energy, Woodhead Publishing, 2017, pp. 179 – 212. doi:10.1016/B978-0-08-100516-3.00009-5.

[7] Y. Yao, Renewable and Sustainable Energy Reviews 58 (2016) 52 – 68. doi:10.1016/j.rser.2015.12.222.

[8] J. Nie, S. Yuan, L. Fang, Q. Zhang, D. Li, Applied Thermal Engineering 129 (2018) 22 – 30. doi:10.1016/j.applthermaleng.2017.09.139.

[9] P. Gao, X. Zhou, B. Cheng, D. Zhang, G. Zhou, International Journal of Heat and Mass Transfer 107 (2017) 916 – 924. doi:10.1016/j.ijheatmasstransfer.2016.11.002.

[10] B. Arun, V. Mariappan, Building Services Engineering Research and Technology 40 (2019) 151–175. doi:10.1177/0143624418810934.

[11] Y. Yao, Y. Pan, S. Liu, Ultrasonics Sonochemistry 62 (2020) 104722. doi:10.1016/j.ultsonch.2019.104722.

[12] J. Ruiz, Experimental characterization and modelling of the binomial distribution system-drift eliminator in cooling towers, Ph.D. thesis, Technical University of Cartagena, 2014.

[13] P. Martínez, J. Ruiz, P. Martínez, A. Kaiser, M. Lucas, Applied Thermal Engineering 138 (2018) 675 – 685. doi:10.1016/j.applthermaleng.2018.04.065.

[14] J. Ruiz, C. Cutillas, A. Kaiser, B. Zamora, H. Sadafi, M. Lucas, Applied Thermal Engineering 149 (2019) 94 – 104. doi:10.1016/j.applthermaleng.2018.12.023.

[15] UNE EN 13741 2004, UNE-EN 13741:2004 Thermal performance acceptance testing of mechanical draught series wet cooling towers, Standard, Spanish Standardization, 2004.

[16] B. N. Taylor, C. E. Kuyatt, Guidelines for Evaluating and Expressing the Uncertainty of NIST Measurement Results, Technical Report, United States Department of Commerce Technology Administration. National Institute of Standards and Technology, 1994. doi:10.6028/NIST.tn.1297.

[17] J. Ruiz, A. Kaiser, M. Ballesta, A. Gil, M. Lucas, Atmospheric Environment 69 (2013) 170 – 181. doi:10.1016/j.atmosenv.2012.12.014.

[18] CTI ATC-140, CTI ATC-140: Isokinetic Drift Test Code, Standard Specifications, Cooling Technology Institute, 1991.

[19] A. Chaskopoulou, M. D. Latham, R. M. Pereira, P. G. Koehler, Journal of the American Mosquito Control Association 29 (2013) 173–176. doi:10.2987/12-6305r.1.

[20] K. Ramisetty, A. Pandit, P. Gogate, Ultrasonics sonochemistry 20 (2012) 254–64. doi:10.1016/j.ultsonch.2012.05.001.

[21] M. Muñoz, S. Goutier, S. Foucaud, G. Mariaux, T. Poirier, Ultrasonics 84 (2018) 25–33. doi:10.1016/j.ultras.2017.10.001.

[22] S. Kooij, A. Astefanei, G. Corthals, D. Bonn, Scientific Reports 9 (2019). doi:10.1038/s41598-019-42599-8.

[23] H. Holterman, Kinetics and evaporation of water drops in air, number 2003-12 in IMAG rapport, IMAG, 2003.

REVIEWER #1 COMMENTS

Reviewer:

The paper presents experimental findings of an ultrasonic mist generator used as an evaporative pre-cooler for condensers in air conditioning applications. It is supported by 23 relevant references. Comments are listed below for consideration.

Authors:

Dear reviewer, we are very grateful to you for your interest and precious comments. They have strengthen the paper considerably. We have addressed all the points raised and provided a suitable reply. Revisions have been made in the new version of the manuscript. We deeply appreciate your consideration of this manuscript.

Reviewer:

- explain how the experimental set up fits the actual installation where the air-condenser is an outdoor unit.

Authors:

As the reviewer points out, one of the challenges faced by the proposed pre-cooling system is its effective implementation in outdoor units subject to the presence of wind. The research stage developed in this paper does not address this issue. This research is focused on the assessment tests of this new system in controlled conditions (wind tunnel), which provides us with experimental data on the thermal and fluid dynamic behaviour of water mist generated by ultrasonic atomization. From this research it is known that, due to the small size of the droplets, the plume of water mist could be carried away by the outside wind. It is therefore important to inject the water mist near the inlet section of the condenser and in a location centred on that section. Furthermore, the conclusions of the study show that it is necessary to increase the dispersion of the plume and the distance covered by the droplets before reaching the condenser, in order to increase the evaporation rate and the pre-cooling effect. In practice, all these conditions can be addressed, for instance, by injecting the water mist in counter-current flow to the inlet air stream of the condenser. Currently, we are immersed in a second stage of research in which we are working to determine the optimal injection geometry, according to the characteristics and power of the condenser. We already have a numerical model in CFD, validated with the results of this article, which is helping us to explore in a simpler way the behaviour of different injection geometries. Figure R1 shows an example of counter-current injection geometry that we are currently testing in a domestic Kaysun branded air conditioning unit with a rated cooling capacity of 2.5 kW.

Reviewer:

- state clearly the actual electric power consumed at different test scenarios.

Authors:

The power consumption in the generation of water mist may be one of the drawbacks of this pre-cooling system. Throughout the tests, measurements of the

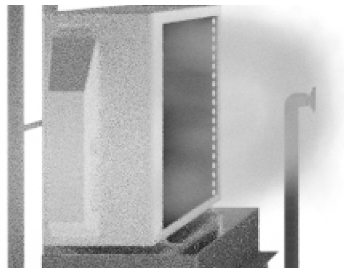

Figure R1: An example of counter-current water mist injection in a domestic condensing unit.

ultrasonic generator's power consumption have been registered. Maximum power consumption of up to 160 W has been observed in tests with higher water mist flow rates. However, this measure of power consumption is not representative of the actual power consumption of an optimized pre-cooling system for a specific condensing unit. In the research stage developed in this study, a commercial water mist generator has been used, which does not allow easy selection of the number of transducers in operation, so it always works with maximum production of atomized water. Tests have shown that a significant amount of atomized water is always wasted, as it accumulates in the atomization chamber without going into the wind tunnel and eventually disappears when it comes into contact with the surface of the water in the tank. There is therefore an energy loss that is difficult to quantify and a power consumption above that of an optimized system, where the number of ultrasonic transducers and the flow rate of water mist are adjusted to the refrigerant capacity of the condenser. For all these reasons these measures have not been included in the article. However, power consumption will be a very important parameter to evaluate in future research work on the real application of this pre-cooling system to different types of aero-condensers. To complement the information on the ultrasonic transducers being used, a table of technical specifications of the mist maker unit has been included, where the maximum consumption per transducer is reported. Please see Table 1.

Reviewer:

- discuss how the technology can be applied to chiller with capacity over, say, 50 TR and how the device can be integrated to the air-cooled condenser.

Authors:

As mentioned in the previous point, this article presents a preliminary phase of research into this pre-cooling system in order to assess its feasibility and performance. We are currently testing domestic air conditioning units, working to optimize the water mist injection geometry. We have already defined some guidelines on how the injection into the condenser should be carried out and we expect to be able to extrapolate to other units with higher capacity and different configuration of the air flow through them.

Reviewer:

- discuss how different climatic conditions influence the mist generator performance.

Authors:

The characteristics of water mist depends on the technical specifications and operating conditions of the ultrasonic atomisation device. The operating conditions that most influence the mist flow rate output (ml/h) and the size of the droplets generated are of an electromechanical nature: input voltage, resonance frequency of the piezo-electric crystal, ceramic disc diameter, water level above the discs, water temperature and physical characteristics of the water (density, dynamic viscosity and surface tension). Ambient temperature and humidity have practically no effect on the droplets generation process and are only significant in the diameter shrinkage of the droplets, once they are introduced into the main airstream of the wind tunnel. The tests presented in this article have been carried out under average environmental conditions similar to the actual conditions in which the real condenser will work (Mediterranean climate). The results obtained under these conditions have been considered adequate for the preliminary research phase of this project. Using a CFD numerical model, the influence of environmental conditions on the evolution of the size and distance travelled by the injected droplets, among other aspects, is currently being studied. As an example, Figure R2 shows the behaviour of the droplet residence time's indicator according to two different ambient conditions. With this indicator it is possible to determine the volumetric rate of droplets that have completely evaporated as a function of the distance covered.

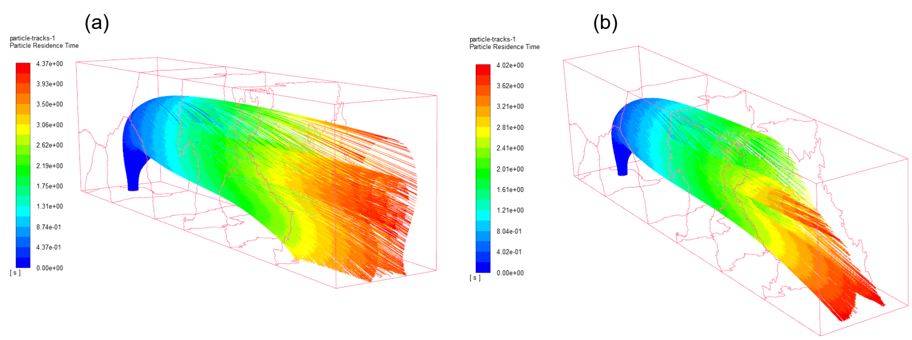

Figure R2: Influence of ambient conditions on droplet residence time: (a) T=20°C, RH=60%; (b) T=30°C, RH=40%.

REVIEWER #3 COMMENTS

Reviewer:

The paper discuss possible application of ultrasonic evaporator in air conditioning system to precool inlet air passing over condenser. Although the idea of ultrasonic evaporator is old but its application as precooling is good.

Authors:

Dear reviewer, we are very grateful to you for your interest and precious comments. They have strengthen the paper considerably. We have addressed all the points raised and provided a suitable reply. Revisions have been made in the new version of the manuscript. We deeply appreciate your consideration of this manuscript.

Reviewer:

However, it is more important to show how this system can be used in specific air conditioning system, and what is the disadvantage of this system compared to other conventional systems, something which is not referred to.

The paper did not discuss the disadvantage of ultrasonic mist generator such ad more power consumption, corrosion, more space and ... and only focused on the general advantages of ultrasonic system.

Authors:

As the reviewer pointed out, one of the most relevant issues for ultrasound pre-cooling to become a commercial product is its coupling to the condenser of the air conditioning system. This is a stage still to be covered since aspects related to the generation of the droplets (number of ultrasonic transducers and their operating conditions) must be optimized, as well as the geometric arrangement of the droplet injections. In addition, there are a number of issues to take into account in this optimization process that today can be considered as disadvantages. One of them is the energy consumption of the ultrasonic mist generation system (if it is not optimized it can be higher than a conventional pad or spray systems). Another issue that can be considered as a disadvantage, in case of not having that precaution in the design, is the possible impact of the droplets on the heat exchanger resulting in corrosion or fouling problems as occurs in conventional spray systems. However, if parameters such as wet length are taken into account in the design, it can be overcome. In general terms, this system will have the same disadvantages as the spray nozzle or deluge systems: corrosion, scaling and fouling phenomena on the heat exchanger bundles. When comparing ultrasonic mist generation to high pressure spray nozzle atomization in pre-cooling applications, the operating costs can be similar. Spray nozzle systems may use less electricity but in most cases are less efficient in evaporation. The spray nozzle systems may operate longer in order to get the same amount of pre-cooling as ultrasonic systems. Droplet size plays a key role in achieving full evaporation and maximum pre-cooling. The smaller the droplet size the faster evaporation occurs. In air conditioning applications, large droplets (spray nozzle) may not evaporate and can collect on coils. Ultrasonic atomization produces smaller droplet sizes for similar power consumption, which is expected to *decrease the severity of these drawbacks: corrosion, scaling and fouling. These ideas regarding the possible disadvantages of ultrasound pre-cooling and the optimization process of its design have been included in the introduction and also in the conclusions section as future work. Please see Section 1, page 4, line 102 and Section 4, page 30, line 598. This article develops a first stage of research in which it is not yet possible to evaluate these disadvantages on an actual air conditioning system. On the other hand, the results of this research are being very useful for the optimization of a pre-cooling system that we are currently testing on a domestic air conditioning system.*

Reviewer:

The experimental results regarding to temperature and humidity measurement in the wind tunnel channel is obvious and there is less interesting findings in this section.

Authors:

Temperature and humidity measurements allow the assessment of the thermal performance of the system and identify problems such as non-uniformity in droplet distribution. They have also been essential to validate a CFD numerical model which is currently being used to investigate other mist injection geometries.

Reviewer:

The location (X & Y) of temperature and humidity probes in the figures should be specified clearly.

Authors:

A new figure has been included in the article with this information. Please see page 6, line 159 and Figure 2.

Reviewer:

There are extra detail regarding the methods which was not appropriate for measurement, which make the text very lengthy. It is better only to name the method which was not successful and concentrate on the method which is used in the work.

Authors:

In the article it was decided to include the detail of all the methods used for the measurement of drop size, with the aim of informing other researchers interested in this matter about which methods do not work in the measurement of drop size, if they are applied in the way we have done. Following the recommendations of the reviewer and in order not to make the text too lengthy, the explanations of the methods which were not appropriate for droplet size measurement have been reduced. Please see Section 3.

REVIEWER #4 COMMENTS

Reviewer:

This paper presents an ultrasonic mist generator, measured the water mist flow, droplet size and distribution, and tested its thermal performance as an evaporative cooler on the self-developed test bench. The uncertainty analysis has been done and the data could be credible. The topic is interesting and the manuscript is well prepared. It is suggested to be accepted for publication after a few modification.

Authors:

Dear reviewer, we are very grateful to you for your interest and precious comments. They have strengthen the paper considerably. We have addressed all the points raised and provided a suitable reply. Revisions have been made in the new version of the manuscript. We deeply appreciate your consideration of this manuscript.

Reviewer:

(1) In general, the manuscript is long and detailed. The abstract and introduction could be concise and compact.

Authors:

Following the reviewer's recommendations, the length of the abstract and introduction has been reduced. Please see Abstract and Section 1.

Reviewer:

(2) Section 2.1, it could be clear to replace lots of words depicting the facility sizes with an annotated sketch.

Authors:

A new figure has been included in the article to show this information more clearly. Please see Figure 2.

Reviewer:

(3) Please indicate the meaning of the subscript number for D1,0,D3,2 D50 ...

Authors:

A new equation has been added in the article with the meaning of the subscript numbers for both the arithmetic and Sauter mean diameters. The median diameter (in terms of droplet count) is now expressed as D_{NM}, to avoid confusion with the subscripts of the previous diameters. Please see Equation 4.

Reviewer:

(4) Section 3.1 and section 3.2, the descriptions for the three measuring techniques and the methods for measuring the mist flow rate are prolix. The words should be succinct, especially for the techniques and methods which were not adopted indeed.

Authors:

In the article it was decided to include the detail of all the methods used for the measurement of both drop size and mist flow rate, with the aim of informing other researchers interested in this matter about which methods do not work in these type of measurements, if they are applied in the way we have done. Following the recommendations of the reviewer and in order not to make the text too lengthy, the explanations of the methods which were not finally adopted have been reduced. Please see Section 3.1 and Section 3.2.

Reviewer:

(5) Figs 9-12, is it possible to compare the temperature or RH curves for a specific transducer in a same coordinate graph?

Authors:

A new figure has been included where you can see the evolution of temperature and relative humidity for the thermo-hygrometer TH2 located at the center of the control section. Please see Figure 14.

Reviewer:

(6) Eqs 9 and 10 are not clear.

Authors:

Below you can see the detailed development of the equations, which has not been included in the article so as not to extend that section:

$\varepsilon_{\mathrm{LCP}}$: local cooling performance

$$\dot{m}_a c_{pma}(T_a - T_{min}) = \dot{m}_w h_{fg}$$
$$c_{pma} = c_{pa} + \omega_a c_{pv}$$
$$\varepsilon_{\mathrm{LCP}} = \frac{T_a - T_{THi}}{T_a - T_{min}} = \frac{T_a - T_{THi}}{\frac{\dot{m}_w h_{fg}}{\dot{m}_a c_{pma}}} = \frac{1}{r_w}\frac{c_{pa} + \omega_a c_{pv}}{h_{fg}}(T_a - T_{THi})$$

where c_{pma} represents the specific heat at constant pressure of moist air (J kg^{-1} K^{-1}).

AER: average evaporation rate

$$\dot{m}_a c_{pma}(T_a - T_{av}) = \dot{m}_{evap} h_{fg}$$
$$(T_a - T_{av}) = \sum_{i=1}^{6}\left(\frac{A_i}{A_T}(T_a - T_i)\right)$$
$$\mathrm{AER} = 100 \times \frac{\dot{m}_{evap}}{\dot{m}_w} = 100 \times \sum_{i=1}^{6}\left(\frac{A_i}{A_T}\frac{1}{r_w}\frac{c_{pa} + \omega_a c_{pv}}{h_{fg}}(T_a - T_i)\right)$$

where T_{av} represents the average temperature of the control section.

Reviewer:

(7) The conclusions should be succinct and highlight the key points. The results from the specific experimental facility but being not universal could be removed.

Authors:

The conclusions have been reordered in order of importance, first highlighting the most relevant results having a more universal character. Please see Section 4

Reviewer:

(8) Lines 639-640, could "no maintenance and cleaning or replacement of the evaporative pads is required" be one of the advantages for the system? As known, nebulization of tap water could produce scale powder, depositing at the surfaces downstream.

Authors:

In principle, this system will have the same disadvantages as the spray nozzle or deluge systems: corrosion, scaling and fouling phenomena on the heat exchanger bundles. However, ultrasonic atomization produces smaller droplet sizes for similar power consumption. The smaller the droplet size the faster evaporation occurs, so it is expected that the severity of these drawbacks will also be reduced. In the case of the evaporative pads, there is an extra problem that consists in the need to replace them periodically, to avoid increasing the pressure loss they produce in the air flow through the condenser, which finally translates into a reduction of the system's COP and an increase in its power consumption. These ideas regarding the possible disadvantages of ultrasound pre-cooling and the optimization process of its design have been included in the introduction and also in the conclusions section as future work. Please see Section 1, page 4, line 102 and Section 4, page 30, line 598.